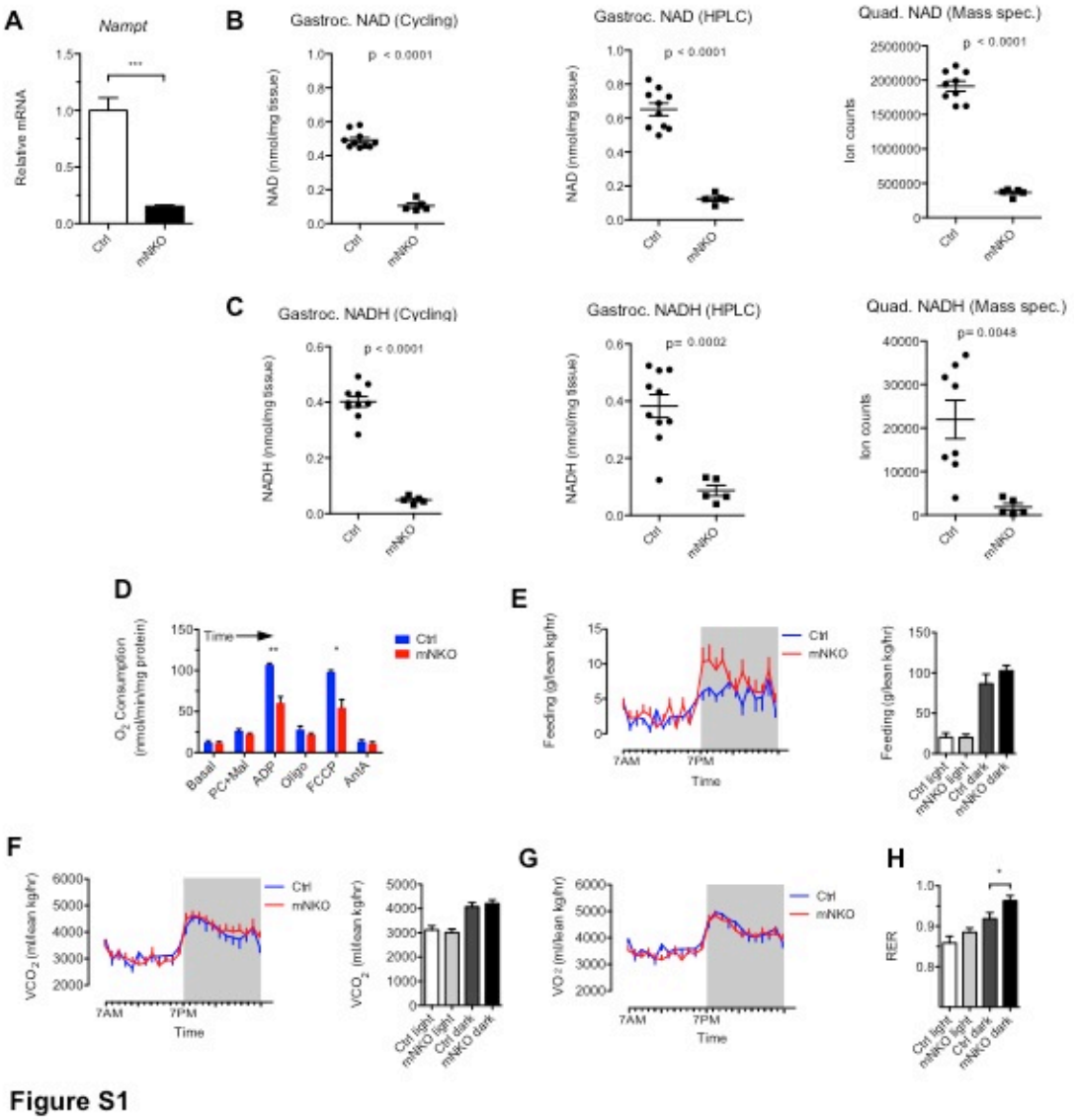

Figure S1

Figure S1. Effects of muscle Nampt deficiency on mitochondrial and whole body respiration and feeding (related to Figure 1)

A, Relative *Nampt* expression in quadriceps muscle normalized to *36B4* (n=4).
B, Validation of techniques used to quantify NAD and
C, NADH in extracts of gastrocnemius (gastroc.) and quadriceps (quad.) muscle by enzymatic cycling assay, HPLC, and mass spectroscopy. Mice were males aged 7 months (n=5-10).
D, Respiratory capacity of isolated muscle mitochondria sequentially provided with palmitoyl carnitine (PC), malate (Mal), and ADP substrates, followed by oligomycin (oligo), FCCP, and antimycin A (AntA)(n=4-6).
E, 24-hour time course and means by light period of food intake,
F, VCO_2, and
G, VO_2 normalized to lean mass (n=7-9).
H, Mean RER during light and dark hours. Error bars represent SEM. Significance was determined by Student's t-test (*p<0.05, **p<0.01). Mice were 3-month-old males unless otherwise indicated.

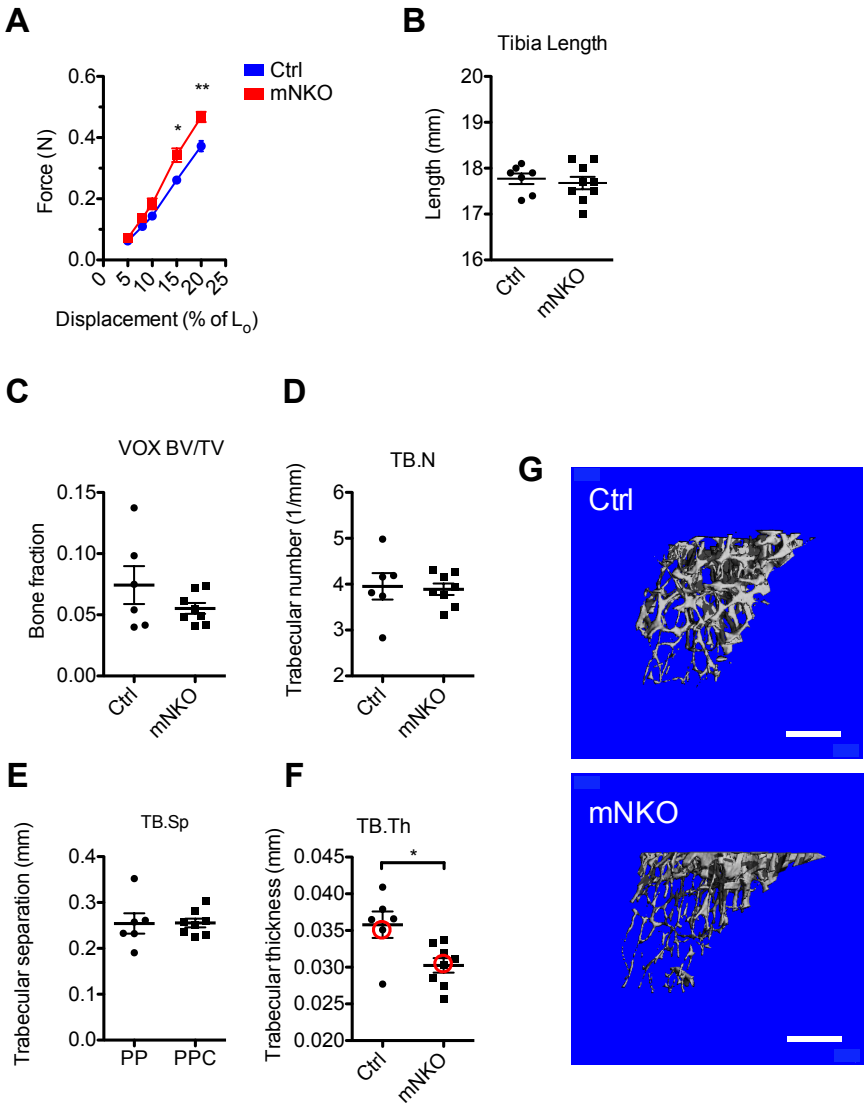

Figure S2

Figure S2. Musculoskeletal features of mNKO mice (related to Figure 2)
A, Resistance to stretch in EDL muscle isolated from 3-month-old mice.
B, Length of tibia bones indicates normal skeletal growth.
C, Relative trabecular bone volume (VOX BV/TV),
D, Number (TB.N),
E, Spacing (TB.Sp), and
F, Thickness (TB.Th) of trabecular plates in metaphysis of tibia bones (n=6-8). Red circles indicate the representative subjects pictured in S2G.
G, Representative three-dimensional reconstructions of trabecular bone. Error bars represent SEM. Scale bars represent 500 µm. Significance was determined by Student's t-test (*p<0.05,**p<0.01). Mice were male aged 3 months.

A

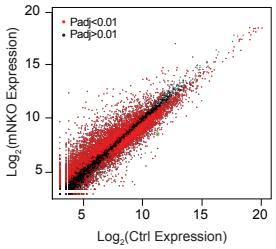

B

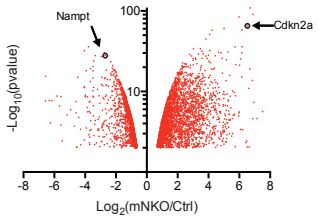

C

Functional Annotation	Predicted Activation State	Activation z-score	p-value
Cell movement of neutrophils	Increased	2.607	8.69E-04
Cell death	Increased	2.46	1.20E-02
Necrosis	Increased	2.265	1.93E-02
Cell rolling of neutrophils	Increased	2.2	8.30E-03
Cell death of muscle	Increased	2.09	1.93E-02
Necrosis of muscle	Increased	2.09	3.32E-02
Force generation of skeletal muscle	Decreased	-2	2.48E-02
Mass of muscle	Decreased	-2.108	5.96E-03
Contractility of muscle	Decreased	-2.182	1.28E-04
Contractility of skeletal muscle	Decreased	-2.515	3.23E-04
Function of skeletal muscle	Decreased	-2.595	1.75E-03

D

Upstream Regulator	Molecule Type	Predicted Activation State	Activation z-score	p-value of Overlap
UCP1	Transporter	Activated	4.329	1.37E-05
SMTNL1	Other	Activated	3.162	1.97E-02
IGF1	Growth factor	-	1.23	7.32E-03
MSTN	Growth factor	-	0.853	1.19E-04
IGF1R	Transmembrane receptor	-	0	2.36E-02
SREBF1	Transcription regulator	-	-0.223	2.04E-02
RORA	Ligand-dependent nuclear receptor	-	-0.577	7.57E-03
AR	Ligand-dependent nuclear receptor	-	-1.414	3.43E-05
FNIP1	Other	-	-1.964	5.51E-02
MED1	Transcription regulator	Inhibited	-2	1.01E-01
COL6A1	Other	Inhibited	-2.137	2.23E-01
STAT5B	Transcription regulator	Inhibited	-2.204	2.48E-04

E

Promoter Motif	p-Value	Target Sequences with Motif	Background Sequences with Motif	Best Match	Score
Upregulated Genes					
	1.00E-26	2.87%	0.61%	SPIC	0.87
	1.00E-17	2.04%	0.49%	STAT1::STAT2	0.84
	1.00E-15	9.69%	5.84%	Znf423	0.66
	1.00E-15	19.36%	13.92%	KLF14	0.91
	1.00E-13	1.14%	0.19%	Hoxa11	0.65
Downregulated Genes					
	1.00E-18	4.87%	1.78%	Stat5a::Stat5b	0.84
	1.00E-18	4.91%	1.83%	RUNX2	0.72
	1.00E-13	0.68%	0.02%	Esrra	0.68
	1.00E-13	13.15%	8.40%	YY1	0.84
	1.00E-12	1.25%	0.19%	EBF1	0.66

Figure S3

Figure S3. Transcriptional and metabolic alterations in mNKO muscle (Related to Figure 3).

A, Scatter plot of RNAseq gene expression profiling in quadriceps muscle from 7-month-old mice (n=4). Red dots indicate significant differences in expression between groups. Specific fold changes and p-values are indicated in Table S1.
B, Volcano plot of genes with significant differential expression in S3A. The *Nampt* and *Cdkn2a* transcripts are indicated.
C, Top biological functions altered in mNKO muscle according to Ingenuity Pathway Analysis of the differentially expressed genes in S3B after filtering for muscle-specific transcripts. Transcripts passing the filter are indicated in Table S1.
D, Predicted upstream regulators of the gene expression pattern identified in S3B according to Ingenuity Pathway Analysis after filtering for muscle-specific transcripts, highlighting Stat5b.
E, Most commonly enriched *de novo* motifs in the promoter regions of the differentially expressed genes in S3B, relative to all mouse promoters. Similarity of identified motifs to those of established transcription factors is indicated, highlighting Stat5b.

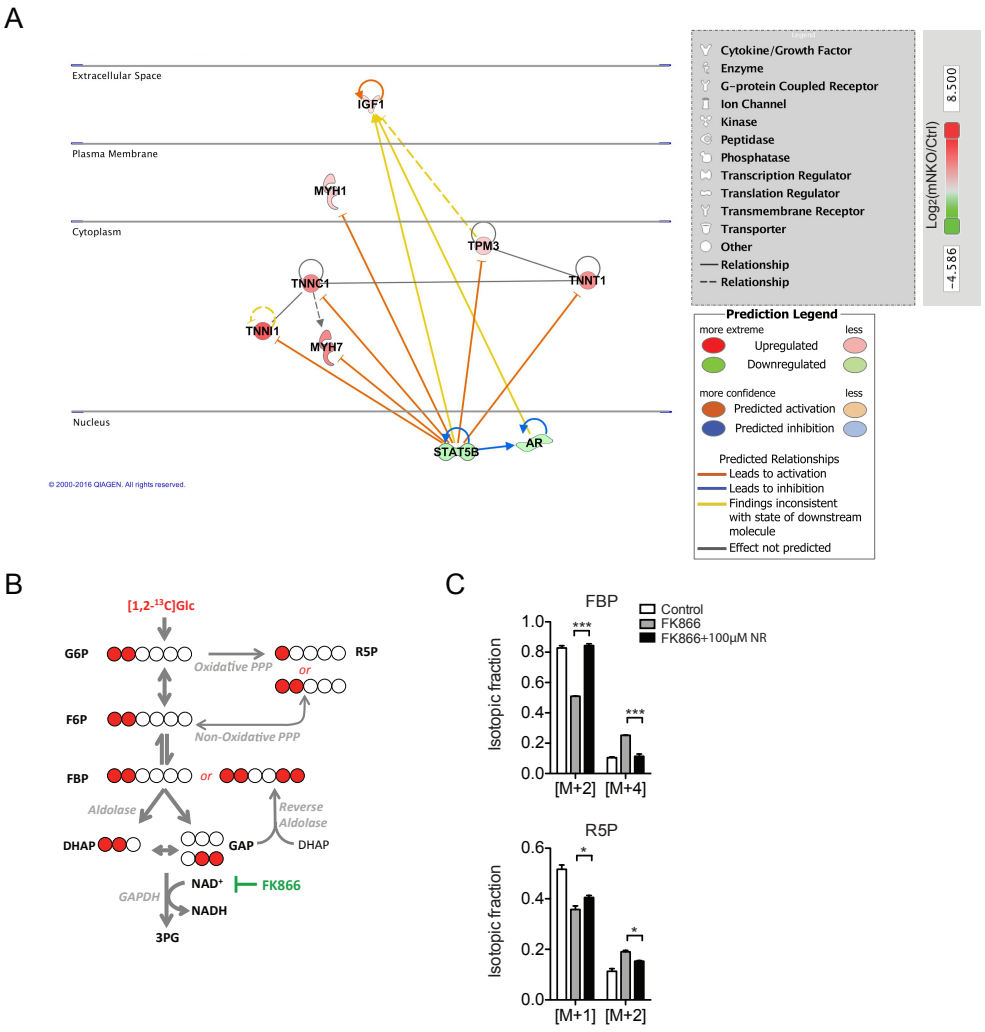

Figure S4

Figure S4. Transcriptional and metabolic alterations in mNKO muscle (Continued, Related to Figure 3).

A, Interaction network of factors identified in B and consistent with inhibition of Stat5b signaling, according to Ingenuity Pathway Analysis. Factors are separated by cellular compartment and colored according to expression level.
B, Schematic representation of ^{13}C isotope incorporation (red circles) into intermediates of the glycolysis and pentose phosphate pathways following addition of [1,2-^{13}C]-glucose to cultured cells. Distinct labeling patterns due to oxPPP activity and aldolase reversal are indicated.
C, Isotope labeling of metabolites in C2C12 myotubes after 12 hours of exposure to [1,2-^{13}C]-glucose. Labeling patterns of fructose-1,6-bisphosphate (FBP) and ribose-5-phosphate (R5P) are represented (n=2-3). Error bars represent SEM. Significance was determined by one-way ANOVA with Tukey post-hoc test (*p<0.05,***p<0.001).

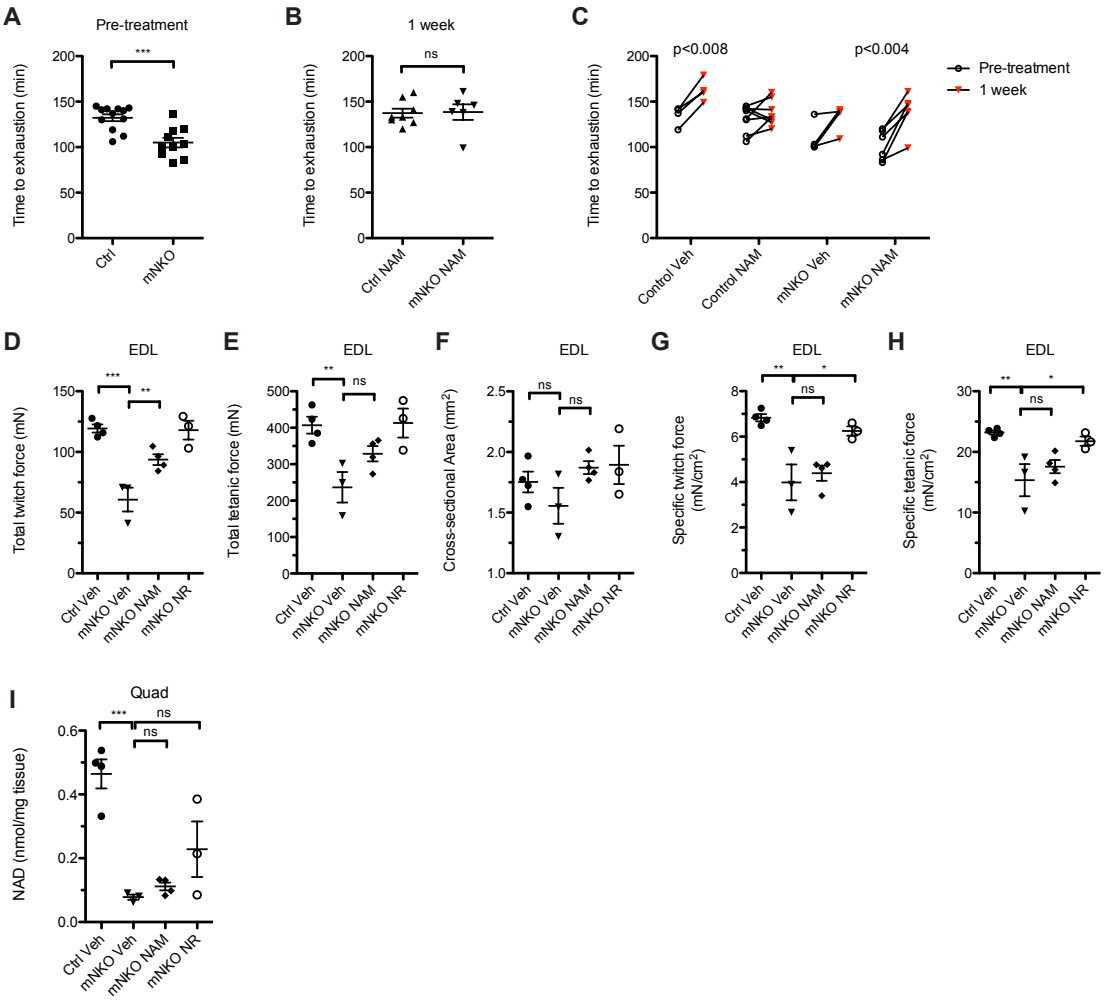

Figure S5

Figure S5. Effects of NAM treatment on mNKO muscle performance (Related to Figure 5).
A, Time elapsed at the point of treadmill exhaustion prior to NAM treatment (n=10-12) and
B, After 1 week of NAM treatment (n=6-8). Significance was determined by unpaired Student's t-test.
C, Change in the exhaustion time of individual mice across one week of NAM treatment, reflecting a training effect in untreated mice (n=4-8).Significance was determined by paired Student's t-test.
D, Maximum total twitch force,

E, Maximum total tetanic force, and
F, Cross-sectional area of isolated EDL muscle after one week of treatment with NAM or NR (n=3-4).
G, Maximum specific twitch force and
H, Maximum specific tetanic force of isolated EDL muscle after one week of treatment (n=3-4).
I, Intramuscular NAD content of quadriceps after one week of treatment (n=3-4). Error bars represent SEM. Unless indicated, significance was determined by one-way ANOVA with Dunnett's post-hoc test compared to mNKO Veh (ns, not significant, *p<0.05,**p<0.01,***p<0.001). All mice were male aged 7 months.

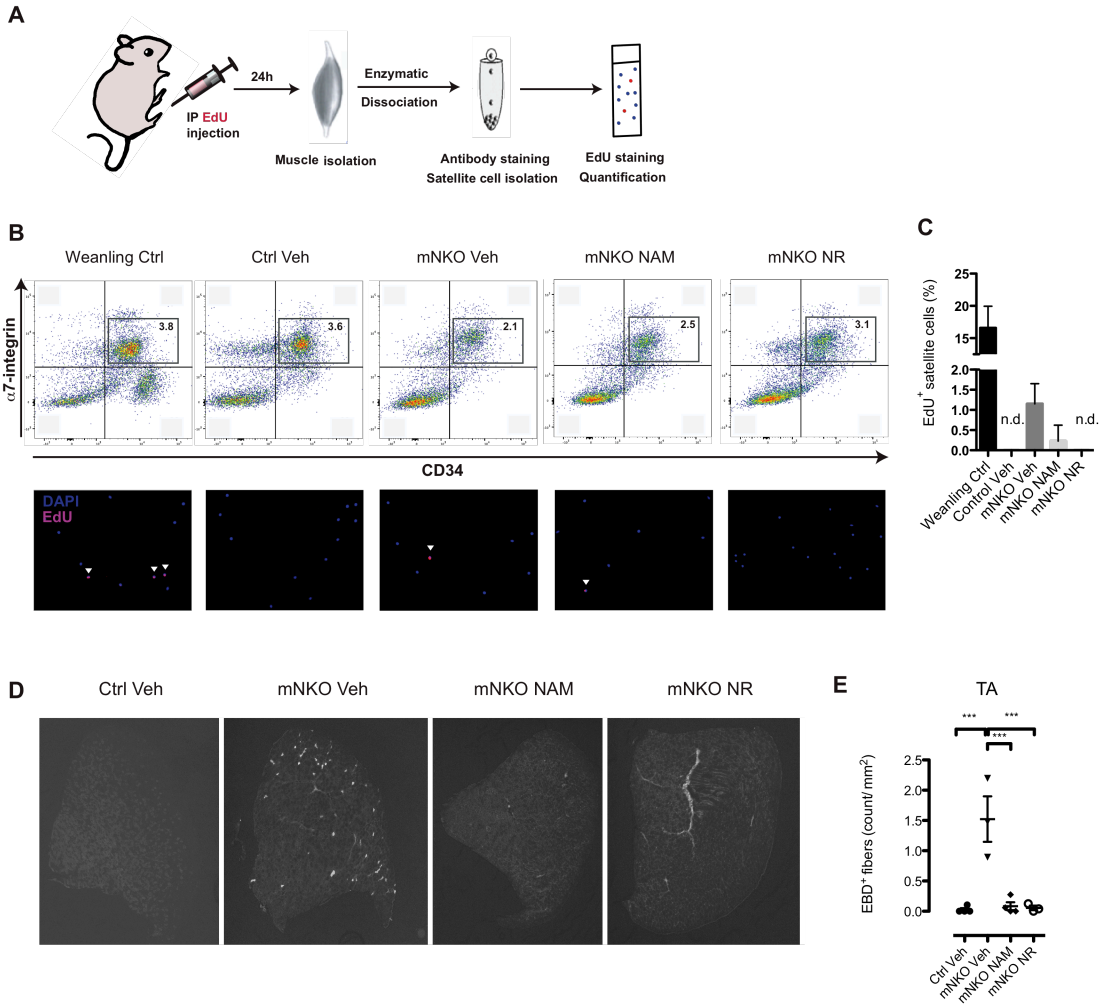

Figure S6

Figure S6. Effects of NAM treatment on mNKO fiber turnover (Related to Figure 5).
A, Schematic of experimental protocol for *in vivo* assessment of muscle satellite cell proliferation from pooled hindlimb muscles. IP, intraperitoneal, EdU, 5-ethynyl-2'-deoxyuridine.
B, Representative scatter plots of FACS-isolated satellite cells (upper panel) and representative images of subsequent immunofluorescence staining from each group (lower panel). Arrowheads indicate EdU+ cells. Scale bar represents 50μm.
C, Proportion of EdU+ satellite cells (N>90 cells from each of 3 animals). N.d., not determined.
D, Representative fluorescent images of EBD uptake into TA muscle 16 hours after IP dye administration.

E, Quantification of EBD positive fibers (n=3). Error bars represent SEM. Significance was determined by one-way ANOVA with Dunnett's post-hoc test compared to mNKO Veh (ns, not significant, *p<0.05,**p<0.01,***p<0.001). All mice were male aged 7 months.

Table S1. Impact of Nampt deletion on the transcriptional profile of skeletal muscle (Related to Figures 3 and S3). Fold changes and p-values are indicated for the transcripts represented in Figure 3A, B and Figure S3A, C.

Table S2. Impact of aging and *Nampt* transgene expression on the transcriptional profile of skeletal muscle (Related to Figure 7). Fold changes and p-values are indicated for each transcript in Figure 7F-H.

Supplemental Experimental Procedures

Calorimetry and body composition

24-hour respiration, locomotion, and feeding activity of individually housed mice was assessed in an open-circuit indirect calorimeter (CLAMS, Columbus Instruments, OH) supplying room air at 0.6 L/min. RER was calculated from the ratio VCO_2/VO_2 and activity was determined by infrared beam breaks. Body composition was determined by nuclear magnetic resonance using a 3-in-1 Analyzer (EchoMRI, Houston, TX) in awake mice.

Histology

EDL and TA muscles were frozen in OCT and cryosectioned at 10 micron thickness. Sections were stained with hematoxilin and eosin (H+E) according to standard procedures. For immunofluorescence, membranes were counterstained with 1:100 dilutions of anti-laminin (L-9393, Sigma) or 1:500 wheat germ agglutinin conjugated to AlexaFluor 647 (Molecular Probes) and nuclei were stained with DAPI. Goat anti-rabbit secondary antibody conjugated to Alexa 488 (Jackson Immunoresearch, West Grove, PA) was diluted 1:500 and incubated for 30 minutes at 37°C. Sections were imaged using an EVOS FL Auto Cell Imaging System (Life Technologies). Analysis of fiber diameter and nuclear position was performed as described using SMASH software, as described previously (Smith and Barton, 2014).

Electron microscopy

EDL muscles that did not undergo the *ex vivo* physiology protocols were maintained at physiological length, fixed with 4% glutaraldehyde in 0.1 M sodium cacodylate buffer (pH 7.2) at room temperature and stored in fixative at 4°C until processed by the Electron Microscopy Resource Laboratory at University of Pennsylvania. Central cross-sectional and longitudinal muscle segments were post-fixed in 2% OsO_4 in cacodylate buffer and embedded. Sections were stained with lead citrate solutions and imaged using a Jeol-1010 Transmission electron microscope.

Bone analysis

Tibia bones were cleaned of connective tissue and fixed in 4% paraformaldehyde overnight at 4°C. Trabecular bone from each metaphysis and cortical bone from each midshaft was selected and scanned at 6 μm resolution using a μCT 35 system (Scanco Medical, Bruttisellen Switzerland). Physical parameters and three-dimensional reconstructions were calculated using associated proprietary software.

Exercise tolerance

Exercise tolerance was assessed using an Exer3-6 treadmill system with shock counter (Columbus Instruments, Columbus OH) running a step-wise accelerating protocol at 0° incline described previously (Frederick, 2015). Mice were habituated to the treadmill at 10 m/min for 15 min 24 hours before and fasted for 3 hours before the experiment. Exhaustion was defined as 50 cumulative stimuli.Lactate was measured from tail blood using a Lactate Pro handheld meter (Arkray, Japan).

Ex vivo muscle physiology

Muscle physiological analysis was performed on isolated EDL muscles using a 1200A Intact Muscle Test

System equipped with Dynamic Muscle Control v.5.415 software (Aurora Scientific, ON, Canada) at the Muscle Physiology Assessment Core of the Pennsylvania Muscle Institute. EDL muscles were dissected and analyzed in constantly oxygenated Ringer's solution (100 mM NaCl, 4.7 mM KCl, 3.4 mM $CaCl_2$, 1.2 mM KH_2PO_4, 1.2 mM $MgSO_4$, 25 mM HEPES, 5.5 mM D-glucose) at 24°C. Maximal isometric twitch and tetanic contractions were obtained using direct electrical field stimulation propagated from two plate electrodes using a frequency of 2500 Hz for 0.2 msec or 120 Hz for 500 msec, respectively. Five minutes were allowed between tests to ensure muscle recovery. Specific force was determined by normalizing absolute force to muscle cros sectional area (CSA). CSA was calculated by dividing the muscle mass by the product of the muscle density coefficient (1.06 g/cm^3), muscle optimal length (L_o), and the fiber length coefficient (0.45 for EDL). Muscle stiffness was measured using a series of passive stretches (10 repetitions per cycle at 2Hz frequency) with increasing amplitude (5, 8, 10, 15, 20% of L_0) performed 5 minutes after the fatigue protocol. The Lissajous curves generated were used to calculate the force opposed by the muscle tissue to the lengthening work (Stedman et al., 1991; Syme, 1990).

Immunoblotting

Frozen tissues were lysed in lysis buffer (25 mM Tris pH 7.9, 100 mM KCl, 5 mM $MgCl_2$, 1% nonidet P-40, 10% glycerol) supplemented with protease inhibitor cocktail (Roche) using a motorized homogenizer. SDS-PAGE was performed on 20 µg of cleared lysate in Laemmli buffer loaded on 10% gels. Gels were transferred to PVDF membranes, blocked in 5% milk, and incubated with 1/1000 dilutions of anti-Nampt (Bethyl A300-372A) and anti-alpha tubulin (Abcam ab40742). Antibody binding was detected and imaged using a chemiluminescent substrate (Perkin Elmer) and Chemi-Doc system (Biorad).

Transcriptome sequencing and analysis

RNA was extracted from quadriceps muscle using the RNeasy fibrous tissue kit (Qiagen) or Trizol reagent (Life Technologies) according to manufacturer protocols. Quantitative PCR to detect *Nampt* and *36B4* transcripts was performed as described (Frederick et al., 2015). Libraries were generated from 1 µg of total RNA using the TruSeq Stranded mRNA Library Prep kit according to the manufacturer's instructions (Illumina). 100 bp single end sequencing was performed on the Illumina HiSeq 2000 at the Next Generation Sequencing Core at the University of Pennsylvania. Reads passing quality filters were trimmed with Cutadapt, mapped to the mouse genome (mm10) with Tophat2, and read counts per gene were determined using HTseq (Anders et al., 2015; Martin, 2011; Trapnell et al., 2009). DEseq2 was used to perform differential expression analysis and to obtain normalized read counts after variance stabilizing transformation as previously described (Ghanem et al., 2015; Love et al., 2014). Normalized read counts were used to generate scatterplots and heatmaps. Genes with an adjusted p-value < 0.01 or <0.05 were considered significant in the mNKO and mNOE samples, respectively. Microarray data for *mdx*mice were obtained from GSE897 using GEO2R and represented in a heatmap generated from genes that were differentially expressed (+/- 2-fold change and p-value < 0.01) in both populations. Gene ontology analysis was performed using the online resource DAVID (Huang et al., 2009a, 2009b). Motif enrichment analysis was performed on promoter sequences from differentially expressed (Padj < 0.05) genes using HOMER (v4.8) with default options (Heinz et al., 2010).Networks were generated through the use of QIAGEN's Ingenuity Pathway Analysis (IPA®) and the Biological Processes and Upstream Regulators were generated through the use of QIAGEN's Ingenuity® iReport (QIAGEN Redwood City, www.qiagen.com/ingenuity).Genes relating to muscle regeneration were described previously (Ryall et al., 2015). All sequencing data generated in this study have been deposited in the USCS genome browser and GEO under the accession number GSE74570.

Cell culture and *in vitro* isotopic labeling

C2C12 myoblasts (ATCC) were cultured in growth medium (20% fetal bovine serum, Gibco). Differentiation was induced by switching the cells to medium containing 2% equine serum (HyClone) supplemented with 1 µg/ml insulin (Sigma), which was changed daily for 3 days. Isotope-labeling medium was prepared from phenol red-, sodium pyruvate-, sodium bicarbonate-free DMEM powder (Cellgro) supplemented with 3.7 g/ L sodium bicarbonate, 25 mM [1,2-^{13}C]glucose (Cambridge Isotope Laboratories) and 4 mM glutamine. Mature myotubes were treated with 100 nM FK866 and either 10 or 100 µM NR. After 2 days, cells were switched to isotope-labeling medium for 12 hours, which was replaced 2 hours before harvesting cells, to ensure steady-state labeling (Munger et al., 2008). Metabolism was quenched and metabolites were extracted by aspirating media and immediately adding 2 mL 80:20

methanol:water on dry ice for 20 min. The resulting mixture was collected and centrifuged at 16,000 xg for 5 minutes. Insoluble pellets were re-extracted with 1 mL 80:20 methanol:water on dry ice. The supernatants from two rounds of extraction were combined, dried under N_2, resuspended in 1 mL water per million cells, and subjected to mass spectrometric analysis. Cell number was determined with an automated cell counter (Invitrogen) and used for normalization of mass spectra.

Metabolite extraction
Metabolites from 50 µl of whole blood were extracted by adding 200 µl ice cold methanol. After 20 minutes of incubation at -20°C and centrifuge at 16,000 xg for 10 min, the resulting supernatant was transferred and insoluble pellets were re-extracted with 1 mL 40:40:20 methanol:acetonitrile:water on ice. The supernatants from two rounds of extraction were combined, dried under N_2, and resuspended in 0.25 mL water. Metabolites for mass spectrometry were extracted from 50 mg of powderized tissues by twice adding 1 ml of dry ice-cooled 80:20 methanol:water with 0.1 % formic acid, incubating for 5 minutes on dry ice, neutralizing with NH_4HCO_3, and centrifuging at 16,000 xg for 10 minutes. Extraction of NADP(H) was achieved with 40:40:20 methanol:acetonitrile:water on ice. The supernatants from two rounds of extraction were combined, dried under N_2, resuspended in 1 mL water, and subjected to mass spectrometric analysis. NADH for enzymatic cycling assays and HPLC was extracted in alkaline buffer (25 mM NH_4Ac, 25 mM NaOH, 50% v/v acetonitrile) and heated at 55°C for 10 minutes, as described previously (Frederick et al., 2015).

HPLC and LC-MS metabolomics
Separation of NAD and NADH in non-diluted extracts by HPLC was performed using an Adsorbosphere XL ODS column preceded by a guard column, as described previously (Frederick et al., 2015). Metabolites for LC-MS were analyzed within 12 hours of extraction by reversed-phase ion-pairing chromatography coupled with negative-mode electrospray-ionization high-resolution MS on a stand-alone orbitrap (Thermo)(Lu et al., 2010). NAM, NMN, NR, and NAD were analyzed by reversed-phase chromatography coupled with positive-mode electrospray-ionization on a Q-Exactive hybrid quadrupole-orbitrap mass spectrometer (Thermo). Liquid chromatography separation was achieved on a Poroshell 120 Bonus-RP column (2.1 mm ×150 mm, 2.7 µm particle size, Agilent). The total run time was 25 minutes with a flow rate of 50 µl/min from 0-12 minutes and 200µl/min from 12-25 minutes, applying a gradient of 0-70 % solvent B (acetonitrile) in 12 min, balanced by solvent A (98:2 water:acetonitrile, 10 mM amino acetate, 0.1 % acetic acid).

Muscle satellite cell isolation and FACS
Gastrocnemius and quadriceps muscles were digested at 37ºC with 0.1% collagenase (Sigma-Aldrich) and 0.4U/mL dispase (Roche). After filtration using a 40 µm cell strainer (Falcon), red blood cells were removed using red cell lysis buffer (eBioscience). Cells were stained with biotinylated antibodies to CD31 (1/200; eBioscience), Sca1 (1/200; BD Pharmingen), CD45 (1/500; BD Pharmingen), and CD11b (1/200; BD Pharmingen), and further stained with antibodies against α-7 integrin (1/25; 647; Ablab), CD34 (1/12.5; BV421; BD Biosciences), and streptavidin PE-Cy7 (1/20; Biolegend). The vital dye 7-AAD (1/250; Sigma-Aldrich) was added and muscle satellite cells (defined as $CD45^-CD11b^-CD31^-Sca1^-CD34^+a7integrin^+$) were sorted on a Becton-Dickinson ARIA II cell sorter equipped with a 100 µm nozzle, as described previously (Sacco et al., 2010).

***In vivo* EdU proliferation assay**
Mice were injected IP with 16 mg/kg EdU 24 hours before cell isolation. Satellite cells were isolated as described above and briefly plated on laminin-coated chamber slides. Cells were processed for EdU incorporation using the Click-iT EdU Plus 594 kit, according to the manufacturer's protocol (Life technologies). Coverslips were mounted using fluoromount G plus DAPI (SouthernBiotech) and cells were imaged with a Nikon Plan Apochromat 10x/0.45 objective on a LSM 710 confocal microscope (Zeiss) using 405nm and 594nm lasers. Images were analyzed using ImageJ.

Supplemental References

Anders, S., Pyl, P.T., and Huber, W. (2015). HTSeq--a Python framework to work with high-throughput sequencing data. Bioinforma. Oxf. Engl. *31*, 166–169.

Frederick, D.W., Davis, J.G., Dávila, A., Agarwal, B., Michan, S., Puchowicz, M.A., Nakamaru-Ogiso, E., and Baur, J.A. (2015). Increasing NAD synthesis in muscle via nicotinamide phosphoribosyltransferase is not sufficient to promote oxidative metabolism. J. Biol. Chem. *290*, 1546–1558.

Ghanem, L.R., Kromer, A., Silverman, I.M., Chatterji, P., Traxler, E., Penzo-Mendez, A., Weiss, M.J., Stanger, B.Z., and Liebhaber, S.A. (2015). The Poly(C) binding protein Pcbp2, and its retrotransposed derivative Pcbp1, are independently essential to mouse development. Mol. Cell. Biol.

Heinz, S., Benner, C., Spann, N., Bertolino, E., Lin, Y.C., Laslo, P., Cheng, J.X., Murre, C., Singh, H., and Glass, C.K. (2010). Simple combinations of lineage-determining transcription factors prime cis-regulatory elements required for macrophage and B cell identities. Mol. Cell *38*, 576–589.

Huang, D.W., Sherman, B.T., and Lempicki, R.A. (2009a). Systematic and integrative analysis of large gene lists using DAVID bioinformatics resources. Nat. Protoc. *4*, 44–57.

Huang, D.W., Sherman, B.T., and Lempicki, R.A. (2009b). Bioinformatics enrichment tools: paths toward the comprehensive functional analysis of large gene lists. Nucleic Acids Res. *37*, 1–13.

Love, M.I., Huber, W., and Anders, S. (2014). Moderated estimation of fold change and dispersion for RNA-seq data with DESeq2. Genome Biol. *15*, 550.

Lu, W., Clasquin, M.F., Melamud, E., Amador-Noguez, D., Caudy, A. a, and Rabinowitz, J.D. (2010). Metabolomic analysis via reversed-phase ion-pairing liquid chromatography coupled to a stand alone orbitrap mass spectrometer. Anal. Chem. *82*, 3212–3221.

Martin, M. (2011). Cutadapt removes adapter sequences from high-throughput sequencing reads. EMBnet.journal *17*, 10.

Munger, J., Bennett, B.D., Parikh, A., Feng, X.-J., McArdle, J., Rabitz, H. a, Shenk, T., and Rabinowitz, J.D. (2008). Systems-level metabolic flux profiling identifies fatty acid synthesis as a target for antiviral therapy. Nat. Biotechnol. *26*, 1179–1186.

Ryall, J.G., Dell'Orso, S., Derfoul, A., Juan, A., Zare, H., Feng, X., Clermont, D., Koulnis, M., Gutierrez-Cruz, G., Fulco, M., et al. (2015). The NAD+-Dependent SIRT1 Deacetylase Translates a Metabolic Switch into Regulatory Epigenetics in Skeletal Muscle Stem Cells. Cell Stem Cell *16*, 171–183.

Sacco, A., Mourkioti, F., Tran, R., Choi, J., Llewellyn, M., Kraft, P., Shkreli, M., Delp, S., Pomerantz, J.H., Artandi, S.E., et al. (2010). Short telomeres and stem cell exhaustion model Duchenne muscular dystrophy in mdx/mTR mice. Cell *143*, 1059–1071.

Smith, L.R., and Barton, E.R. (2014). SMASH – semi-automatic muscle analysis using segmentation of histology: a MATLAB application. Skelet. Muscle *4*, 21.

Stedman, H.H., Sweeney, H.L., Shrager, J.B., Maguire, H.C., Panettieri, R.A., Petrof, B., Narusawa, M., Leferovich, J.M., Sladky, J.T., and Kelly, A.M. (1991). The mdx mouse diaphragm reproduces the degenerative changes of Duchenne muscular dystrophy. Nature *352*, 536–539.

Syme, D.A. (1990). Passive viscoelastic work of isolated rat, Rattus norvegicus, diaphragm muscle. J. Physiol. *424*, 301–315.

Trapnell, C., Pachter, L., and Salzberg, S.L. (2009). TopHat: discovering splice junctions with RNA-Seq. Bioinforma. Oxf. Engl. *25*, 1105–1111.